

# An Improved Hierarchical ACA Technique for Sound Absorbent Materials

A. Brancati<sup>1</sup>, M. H. Aliabadi<sup>1</sup> and A. Milazzo<sup>2</sup>

**Abstract:** This paper presents an improved adaptive cross approximation (ACA) approach developed in conjunction with the Hierarchical format matrix and the GMRES solver. A novel scheme to generate the cluster tree (based upon preliminary considerations of the prescribed boundary conditions) and an improved ACA algorithm (approximating the system matrix for mixed Robin conditions) are described. The asymptotic smoothness property of a kernel generated by a linear combination of two asymptotic smooth kernels is demonstrated. Numerical results show the new approach to be up to 50% faster than the conventional ACA approach.

## 1 Introduction

There are several techniques for solving both internal and external acoustic problems, but the most popular and efficient methods for engineering analyses are the Finite Element Method (FEM) and the Boundary Element Method (BEM) [Wrobel and Aliabadi (2002)]. The main advantage of the BEM over the FEM is related to the reduction in modelling effort. The FEM discretisation includes the whole domain of the problem, while the BEM requires only the discretisation of the boundary. Hence, the FEM can not be directly utilised for unbounded problems and it leads to larger system matrix than the BEM, but symmetric, sparse and banded, that grows almost linearly with the size of the problem. On the contrary, boundary element matrices are non-symmetric and fully populated, and its memory storage requirement is of  $O(N^2)$ , with  $N$  being the number of degrees of freedom (d.o.f.). Typically direct solvers require  $O(N^3)$  operations while iterative solvers  $O(kN^2)$ , where  $k$  is the number of iterations.

The above drawbacks reduce the efficiency of the BEM. In this regard, several techniques have been developed to reduce the memory storage requirements and the

---

<sup>1</sup> Department of Aeronautics, Imperial College London, South Kensington, SW7 2AZ

<sup>2</sup> Dipartimento di Ingegneria Civile, Ambientale e Aerospaziale, Facoltà di Ingegneria, Università degli Studi, Palermo

CPU solution time. They include: block equation solvers [Crotty (1982)], multi-zone boundary element analyses [Rigby and Aliabadi (1995); Kane and Kumar (1990)], iterative techniques [Mansur, Araújo and Malaghini (1992)], panel clustering [Hackbusch and Nowak (1989)]. However, the techniques that exhibit the most effective computational benefits in solving acoustic simulations are the fast multiple method (FMM) [Carrier, Greengard and Rokhlin (1988); Greengard and Rokhlin (1987); Rokhlin (1983); Wang and Yao (2008)] and, more recently, the adaptive cross approximation (ACA) [Bebendorf (2000); Bebendorf and Rjasanow (2003)]. Although the FMM is known to be a fast and efficient technique for BE problems, it is based on the expansion of the kernels and its terms are required to be evaluated several times during the solution process and then integrated, which can lead to significant changes of standard BEM codes. Similarly, the ACA reduces the computational costs by expanding the kernel, but the expansions are calculated by existing kernels, which means that a block of the solving matrix is approximated by evaluating only a few entries of the original block (see figure 1). By this technique the whole matrix is divided into two groups of blocks, the *full rank* blocks, represented entirely, and the *low rank* blocks that allow the ACA approximation achieving approximately  $O(N)$  for both storage and matrix-vector multiplication [Benedetti, Aliabadi and Daví (2007); Hackbusch and Nowak (1989)].

Several authors have compared the efficiency of the two techniques (see for instance [Wang, Hall, Yu, and Yao (2008); Buchau, Rucker, Rain, Rischmüller, Kurz and Rjasanow (2003)]). It is not possible to select a technique having the best performances for all types of problems. ACA is much better suited to types of problems where repeated matrix-vector multiplication is required such as optimisation problems and simulations where frequency is close to its upper limit of applicability for a given mesh.

since the FMM is well suited for solving large scale problems in a conventional computer, whereas the ACA is ideal for solution with numerous matrix-vector multiplication such as optimisation problems and simulations where frequency is close to its upper limit of applicability for a given mesh.

The hierarchical matrix ( $\mathcal{H}$ -matrix) format has been proposed by [Hackbush (1999); Hackbush and Khoromskij (2000)] to accelerate the matrix-vector product of discrete integral operators and it has been previously utilised in conjunction with the ACA by several authors [Benedetti, Aliabadi and Daví (2007); Börm and Grasedyck (2000); Benedetti and Aliabadi (2010); Brancati and Aliabadi (2011); Brancati, Aliabadi and Mallardo (2011)].

The superiority of iterative solvers over direct solvers it is well known and much effort has been spent to investigate solvers for non symmetric linear systems. One of the most popular techniques is the generalized minimal residual method (GM-

RES) originally proposed by [Saad and Schultz (1986)] and further developed by other authors [Leung and Walker (1997); Merkel, Bulgakov, Bialecki and Kuhn (1998)].

This paper presents a novel BEM approach based on the  $\mathcal{H}$ -matrix, the ACA and the GMRES. The authors' previous formulation [Brancati, Aliabadi and Benedetti (2009)] has been improved to reduce the CPU time significantly, compared with conventional BE methods, for solving sound propagation problems with mixed boundary conditions. The improved approach is presented giving detailed description of procedure for generating the cluster tree. Also demonstrated is that the linear combination of two asymptotic smooth kernels (with respect to the collocation point only) generates an asymptotic smoothness kernel. Comparison with the standard ACA shows that a 40% higher reduction on the CPU time and memory storage requirement can be achieved, allowing to solve larger scales problems, particularly in case of mixed Robin boundary conditions.

## 2 The Boundary Elements Method for the Helmholtz Equation

In general acoustic simulations, the field is formulated using the linear wave equation that in case of time-harmonic wave motion the solution can be evaluated as the product of two functions, the first depends only upon the space, i.e. the velocity potential  $u(\mathbf{X})$ , here referred simply to potential, and the second only upon the time, i.e.  $e^{i\omega t}$ . Due to this hypothesis the acoustic field can be described by the Helmholtz equation valid at each point  $\mathbf{X}$  of the domain

$$\nabla^2 u(\mathbf{X}) + k^2 u(\mathbf{X}) = \frac{1}{c^2} b \quad (1)$$

where  $u(\mathbf{X})$  is the potential,  $\nabla^2$  is the Laplacian operator,  $k = \omega/c$ , with  $c$  sound velocity and  $\omega$  angular frequency, is the wave number. The last term of the equation above refers to the presence of sources within the domain with strength  $b$ .

In acoustics, the boundary conditions (BCs) can be divided into three groups as follows

$$u(\mathbf{x}) = \bar{u}(\mathbf{x}) \quad \mathbf{x} \in \Gamma_1 \quad (2a)$$

$$q(\mathbf{x}) = u(\mathbf{x})_{,n} = \bar{q}(\mathbf{x}) \quad \mathbf{x} \in \Gamma_2 \quad (2b)$$

$$\bar{\alpha}u(\mathbf{x}) + \bar{\beta}q(\mathbf{x}) = \bar{\gamma} \quad \mathbf{x} \in \Gamma_3 \quad (2c)$$

where  $\Gamma_1$ ,  $\Gamma_2$  and  $\Gamma_3$  are three non-intersecting surfaces such that  $\Gamma_1 \cup \Gamma_2 \cup \Gamma_3 = \Gamma$ ,  $\mathbf{x}$  is a boundary point,  $\mathbf{n}(\mathbf{x})$  is the outward normal to the boundary.

When modelling real problems, the main goal is the evaluation of the sound pressure level (SPL) at selected points for a discrete number of frequencies where acoustic sources, such as monopoles or planewaves, perturb the air inside an enclosed space or around a certain object whose surfaces have a predefined value of absorbing coefficient (or impedance). Hence, the first two BCs, called Dirichlet (2a) and Neumann (2b), respectively, are quite rare and they represent, under certain conditions, hard, soft and vibrating surfaces. Most common absorbing materials are mathematically described with the third group of BCs, namely mixed Robin conditions. Relationship (2c) can be also expressed as follows

$$q(\mathbf{x}) = \frac{p(\mathbf{x})}{z(\mathbf{x})} = -i\rho\omega \frac{u(\mathbf{x})}{z(\mathbf{x})} \quad (3)$$

where  $q$  is the potential gradient,  $p$  is the pressure,  $\rho$  is the density of the medium and  $z$  is the specific surface impedance.

The absorbing coefficient of materials can be connected to the impedance value  $z$  as suggested by Mallardo *et al.* Mallardo, Aliabadi, Brancati and Marant (2011).

The conventional BEM formulation for acoustic simulations relates the values at the boundary  $\Gamma$  of the potential  $u(\mathbf{x}')$  with its gradient, the flux  $q(\mathbf{x}')$ , as follows

$$c(\mathbf{x}')u(\mathbf{x}') = \int_{\Gamma} u^*(\mathbf{x}', \mathbf{x})q(\mathbf{x})d\Gamma - \int_{\Gamma} u(\mathbf{x})q^*(\mathbf{x}', \mathbf{x})d\Gamma \quad (4)$$

where  $u^*(\mathbf{x}', \mathbf{x})$  and  $q^*(\mathbf{x}', \mathbf{x})$  are the potential and flux fundamental solutions, respectively, and  $c(\mathbf{x}')$  is a coefficient related to the smoothness properties of the boundary at the point  $\mathbf{x}'$  (see [Wrobel and Aliabadi (2002)]).

The exact solution of the equation (4) is analytically evaluated only for a few problems with simple geometries. Complex geometries require a numerical method that requires the discretisation of the geometry using shape functions or interpolating function. In the present study the superparametric formulation using constant unknown and linear geometry elements is adopted. Equation (4) is then transformed to a system of  $N$  algebraic equations, where  $N$  is the number of degrees of freedom of the problem, that can be written under the following matrix notation

$$\mathbf{H}\mathbf{u} = \mathbf{G}\mathbf{q} + \mathbf{p} \quad (5)$$

The coefficient matrices  $\mathbf{H}$  and  $\mathbf{G}$  are both  $N \times N$  and they are evaluated by the integrals of the product between the Jacobian of transformation with flux and potential fundamental solutions, respectively. The boundary quantities in terms of potential and flux are collected by two  $N \times 1$  vectors,  $\mathbf{u}$  and  $\mathbf{q}$ , respectively. The

last term  $\mathbf{p}$  refers to the effect due to the presence of sources, such as monopoles and planewaves, inside the domain  $\Omega$  of the problem.

By applying the BCs, the following system of algebraic equations is obtained

$$\mathbf{A}\mathbf{Y} = \mathbf{F} \quad (6)$$

where  $\mathbf{Y}$  is a  $N \times 1$  vector that collect all the unknowns of the problem,  $\mathbf{A}$  is a  $N \times N$  matrix composed by the columns of  $\mathbf{H}$  and  $\mathbf{G}$  that correspond to the unknowns, and  $\mathbf{F}$  is a  $N \times 1$  vector evaluated by multiplying the columns of  $\mathbf{H}$  and  $\mathbf{G}$  by the corresponding BCs and it may include the effect of extra sources inside the domain. The potential  $\mathbf{U}$  at selected internal points is evaluated by a post processing step where the potential and flux vectors are required

$$\mathbf{U} = -\overline{\mathbf{H}}\mathbf{u} + \overline{\mathbf{G}}\mathbf{q} + \mathbf{P} \quad (7)$$

where  $\overline{\mathbf{H}}$  and  $\overline{\mathbf{G}}$  are two coefficient matrices similar to  $\mathbf{H}$  and  $\mathbf{G}$ , but evaluated at internal point, and  $\mathbf{P}$  refers to the presence of sources inside the domain.

### 3 Hierarchical-ACA

This section presents a brief introduction to the hierarchical matrix ( $\mathcal{H}$  – matrix) format, originally introduced by [Hackbush (1999); Hackbush and Khoromskij (2000)], and to the Adaptive Cross Approximation (ACA) [Bebendorf (2000); Bebendorf and Rjasanow (2003)].

The  $\mathcal{H}$  – matrix format is a powerful mathematical instrument that, in conjunction with the ACA and iterative solvers, allows a significant reduction to the solution time due to three main factors, i.e., the hierarchical partitioning of the matrix into blocks, the block-wise restriction of approximated blocks (see figure 1) and the matrix-vector multiplication with almost linear complexity.

The whole matrix is divided into two classes of blocks: some of them are represented entirely (*full rank* blocks), whereas some others allow a special representation (*low rank* blocks). In this study, the latter blocks are approximated by the ACA, an approach consisting on calculating only a few coefficients of the original block to reproduce the whole block.

A block ( $\beta_{ij}(\mathbf{x}'_i, \mathbf{x}_j)$ ) contained in the system matrix is constituted by a series of coefficients that are evaluated by an integration process of the kind

$$\beta_{ij}(\mathbf{x}'_i, \mathbf{x}_j) = \int_{\Gamma_i} \kappa^*(\mathbf{x}'_i, \mathbf{x}_j) \varphi(\mathbf{x}_j) d\Gamma_i \quad (8)$$

where  $\mathbf{x}'_i$  is the  $i$  – th collocation node,  $\mathbf{x}_j$  is the node of the field elements  $\Gamma_i$ ,  $\kappa^*(\mathbf{x}'_i, \mathbf{x}_j)$  is the block kernel and  $\varphi(\mathbf{x}_j)$  represent the generic values of potential or flux at the point  $\mathbf{x}_j$ , or shape functions.



BCs. This procedure allows to eliminate the computational costs related to the evaluation of the missing pieces of information in case a block tree has an element with a different BC from the predominant BCs of that block [Brancati, Aliabadi and Benedetti (2009)]. In the following hierarchical partition a geometrical criterion is adopted as in conventional approaches.

In acoustic simulations there are three possible BCs (potential, flux and impedance), whereas the cluster tree is well known to be a binary tree. To overcome this difficulty, the initial set of the tree  $I = \{1, 2, \dots, N\}$  (namely *root of the tree*) with  $N$  denoting the total number of elements, is split into two subsets (called *sons*) collecting elements with BCs expressed in terms of: *i*) impedance and *ii*) potential and flux. Then, the latter subset is further split to collect *i*) purely potential and *ii*) purely flux BCs, respectively. Figure 2 shows the partition that is obtained in case of presence of all three BCs at the same time.

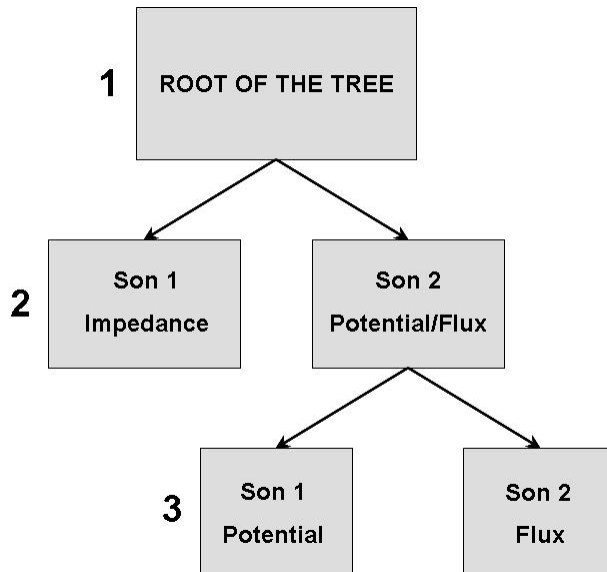


Figure 2: Representation of the first two iterations of the cluster tree creation: 1) the whole geometry is divided 2) into two parts, based on the BCs: Son1 Impedance; Son2 Potential/flux. Son2 is then subdivided again 3) to consider elements with pure potential (Son1) and flux (Son2) BCs.

Next, the procedure follows the conventional partition to group together contiguous nodes and elements with same BCs. The set  $I_i = \{1, 2, \dots, n_i\}$  of each group, with  $n_i$  denoting the number of elements contained into each subset, is split, using a

specific criterion, into pairwise disjoint subsets. The criterion adopted here is based on a geometric criterion based upon the distance between collocation points and field points: a subset is split into two subsets along the maximum extension of the geometry using its middle point. Each of this subset is afterward split in two other subsets following this criterion recursively, until the number of the elements below a certain value, called here *cardinality* [Benedetti, Aliabadi and Daví (2007)].

### 3.2 Block Tree

The block tree is generated after the cluster tree is set. The binary cluster tree subdivides the index set  $I$  of the basic matrix indexes  $I \times I$ . The solving matrix is hierarchical partitioned and all blocks are classified into two different groups, full rank blocks, represented entirely, and low rank blocks, that have an approximated representation. This classification is accomplished with the assistance of a geometrical criterion based on the distance  $dist$  and diameter  $diam$  between a group of elements ( $\Omega_r$ ) and a group of nodes ( $\Omega_c$ ) as follows

$$\min(diam \Omega_c, diam \Omega_r) \leq \eta dist(\Omega_c, \Omega_r) \quad (9)$$

where  $\eta$  is a fundamental parameter that influences the convergence and the acceleration ratio of the whole procedure [Brancati (2010)]. In the present study  $\eta$  is equal to 50.

The diameter of each of the two groups and their distance are not evaluated exactly, but considering the box that contains each of this group whose corner points are easily evaluated by the maximum and minimum coordinates of the points inside the box along the three axes ( $x_1, x_2, x_3$ ).

The block tree is a quaternary tree and it cannot be used directly when the presented cluster tree is adopted. The proposed strategy to overcome this problem is represented in figure 3. The first step divides the solving matrix into four blocks based upon the previously generated cluster tree. The first two blocks (“11” and “12”) are already constituted by all elements with the same impedance BCs, hence their subdivision can follow directly the conventional procedure [Benedetti, Aliabadi and Daví (2007)], whereas the other two blocks (“22” and “21”) need to be further split by a non-standard technique to keep into account the potential and flux BCs.

### 3.3 ACA

The ACA was originally introduced by Bebendorf [Bebendorf (2000)]. It is based on the consideration that the kernels  $\kappa(\mathbf{x}', \mathbf{x})$  of a group of contiguous field and collocation points can be approximated by an expansion as follows [Bebendorf and

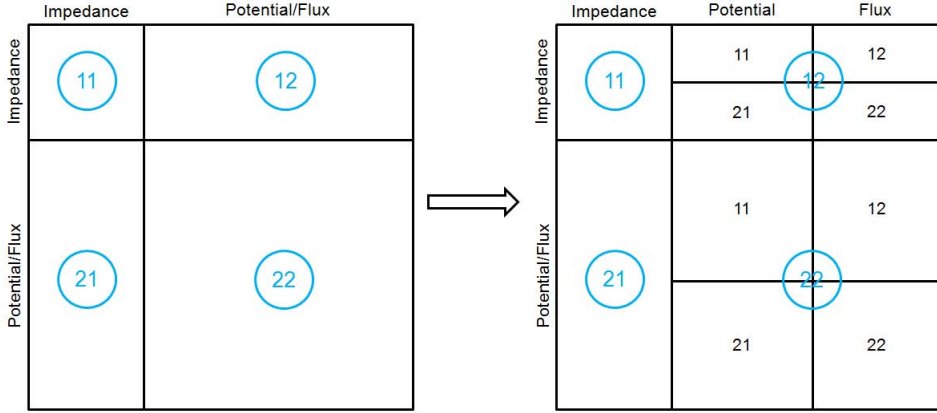


Figure 3: Representation of the first two iterations of the block tree creation.

Rjasanow (2003)]

$$\kappa(\mathbf{x}', \mathbf{x}) = \sum_{i=1}^k v_i^*(\mathbf{x}') w_i(\mathbf{x}) + R_k(\mathbf{x}', \mathbf{x}) \quad (10)$$

where the two functions  $v_i^*(\mathbf{x}')$  and  $w_i(\mathbf{x})$  depend only upon the collocation points and the field points, respectively, and  $R_k(\mathbf{x}', \mathbf{x})$  is the residuum that tends to zero when  $k$  tends to the rank of the original block. It should be noted that for the ACA the functions  $v_i^*$  and  $w_i$  are the  $i$ -th row and column of the block under analysis.

The necessary and sufficient condition for the existence of the low rank approximants is the asymptotic smoothness of the kernel  $\kappa(\mathbf{x}', \mathbf{x})$  with respect to  $\mathbf{x}'$  (not with respect to  $\mathbf{x}$ ) [Bebendorf and Rjasanow (2003); Bebendorf and Grzhibovskis (2006)].

The kernel  $\kappa(\mathbf{x}', \mathbf{x})$  is defined asymptotically smooth with respect to  $\mathbf{x}'$  if there are two constants  $c_p > 0$  and  $g < 0$  so that for any multiindex  $\alpha \in \mathbb{N}_0^n$  it holds the following

$$|\kappa_{,\mathbf{x}'}^\alpha(\mathbf{x}', \mathbf{x})| \leq c_p |\mathbf{x}' - \mathbf{x}|^{g-p}, \quad p = |\alpha| \quad (11)$$

where  $c_p$  depends only upon  $p$  and where  $\cdot_{,\mathbf{x}'}$  denotes the derivative with respect to the collocation point

$$\cdot_{,\mathbf{x}'}^\alpha(\mathbf{x}', \mathbf{x}) = \left( \frac{\partial}{\partial \mathbf{x}'} \cdot (\mathbf{x}', \mathbf{x}) \right)^\alpha \quad (12)$$

The potential and flux fundamental solutions satisfy the relation (11) [Von Estorff, Rjasanow, Stolper and Zalesk (2005)]

$$\left| \left( u_{,\mathbf{x}'}^*(\mathbf{x}', \mathbf{x}) \right)^\alpha \right| \leq c_{pu} |\mathbf{x}' - \mathbf{x}|^{g_u - P} \quad (13)$$

$$\left| \left( q_{,\mathbf{x}'}^*(\mathbf{x}', \mathbf{x}) \right)^\alpha \right| \leq c_{pq} |\mathbf{x}' - \mathbf{x}|^{g_q - P}$$

where  $c_{pu}$  and  $g_u$  refer to the potential fundamental solution, and  $c_{pq}$  and  $g_q$  to the flux fundamental solution.

The asymptotic smooth property holds also for a linear combination of the potential and flux fundamental solutions

$$f^*(\mathbf{x}', \mathbf{x}) = u^*(\mathbf{x}', \mathbf{x}) + \zeta q^*(\mathbf{x}', \mathbf{x}) \quad (14)$$

with  $\zeta = \frac{i\rho\omega}{z}$  a complex constant. To demonstrate the above observation, let us consider the linear combination of the both relations in (13) for which it holds

$$\begin{aligned} \left| \left( f_{,\mathbf{x}'}^*(\mathbf{x}', \mathbf{x}) \right)^\alpha \right| &\leq \left| \left( u_{,\mathbf{x}'}^*(\mathbf{x}', \mathbf{x}) \right)^\alpha \right| + \left| \zeta \left( q_{,\mathbf{x}'}^*(\mathbf{x}', \mathbf{x}) \right)^\alpha \right| \\ &\leq c_{pu} |\mathbf{x}' - \mathbf{x}|^{g_u - P} + \zeta c_{pq} |\mathbf{x}' - \mathbf{x}|^{g_q - P} \end{aligned} \quad (15)$$

Now, it is evident that

$$\left| \left( f_{,\mathbf{x}'}^*(\mathbf{x}', \mathbf{x}) \right)^\alpha \right| \leq c_{pf} |\mathbf{x}' - \mathbf{x}|^{g_f - P} = (\beta c_{pu} + \zeta c_{pq}) |\mathbf{x}' - \mathbf{x}|^{g_q - P} \quad (16)$$

where

$$\beta = |\mathbf{x}' - \mathbf{x}|^{g_u - g_q} \quad (17)$$

In conclusion the two constants  $c_{pf}$  and  $g_f$  can be evaluated by  $c_{pu}$ ,  $c_{pq}$ ,  $\beta$  and  $\zeta$ , whereas  $g_q = g_f$ .

### 3.3.1 Stopping criterion

Equation (10) can be seen in a matrix format by considering a generic admissible  $m \times n$  block,  $\mathbf{C}_a$ , and an approximating block,  $\mathbf{C}_k$ , constituted by  $k$  columns  $\mathbf{a}_i$  and  $k$  rows  $\mathbf{b}_i$  as follows

$$\mathbf{C}_a \simeq \mathbf{C}_k = \sum_{i=1}^k \mathbf{a}_i \mathbf{b}_i^T \quad (18)$$

with  $k \ll m$  and  $k \ll n$  rank of the low rank block. The block  $\mathbf{C}_k$  approximates the block  $\mathbf{C}_a$  with a selected accuracy  $\varepsilon$ , such that

$$\|\mathbf{C}_a - \mathbf{C}_k\|_F \leq \varepsilon \|\mathbf{C}_a\|_F \quad (19)$$

where  $\|\cdot\|_F$  stands as the *Frobenius norm*. In this study  $\varepsilon$  is set equal to  $10^{-5}$ . A higher level of accuracy is achieved by increasing the number of entries, hence, the rank of the block  $\mathbf{C}_k$ . This is the reason why the approach is called “adaptive”.

Relation (19) is the necessary condition to achieve a certain level of accuracy used by the fully pivoted ACA. As evident the value of an entire admissible block  $\mathbf{C}_a$  is always required. In this contribution, a partially pivoted ACA is preferred instead, and the above relationship is substituted by

$$\sqrt{(\mathbf{a}_k \cdot \mathbf{a}_k^*) (\mathbf{b}_k \cdot \mathbf{b}_k^*)} \leq \varepsilon \quad (20)$$

where  $\mathbf{a}_k$  and  $\mathbf{b}_k$  represent the column and row computed at the  $k - th$  iteration, and  $\mathbf{a}_k^*$  and  $\mathbf{b}_k^*$  their complex and conjugate, respectively.

It is possible that the rank of a few admissible blocks correspond to the original matrix rank. In this eventuality such blocks occupy the double the memory of a full rank block, thus in the proposed procedure such blocks are eliminated and substituted by conventional full rank blocks.

### 3.4 $\mathcal{H}$ -Matrix Format

The structure of the  $\mathcal{H}$ -matrix format was originally developed to reduce the computational cost of the building process and the matrix-vector multiplication of discrete integral operators with smooth kernels, such as in the BE formulation. More details on this regards are given in [Hackbush (1999); Hackbush and Khoromskij (2000)].

A conventional matrix-vector product requires  $m(2n - 1)$  operations, whereas using the  $\mathcal{H}$ -matrix format they are  $m(2k - 1) + k(2m - 1)$ . Hence, the approach permits to reduce the number of operations only if the following relation holds

$$k_h < \frac{2m(n - 1)}{2(m + n) - 1} \quad (21)$$

In general  $k$  is much less than this upper limit, especially if the separation distance between two groups of collocation and field points is great.

It should be noticed that relation (21) can be selected as an optimised and alternative stopping criterion to the conventional one. In fact, an admissible block with rank superior than  $k_h$  needs a larger number of operations to evaluate the matrix-vector product than a full rank block and it slows down the iterative solver. In this case it strongly recommended to use a conventional representation instead than the ACA.

Additionally, the ACA algorithm can be optimised for all those blocks constituted by all zero coefficients, that are not so rare in solving 3D linear Helmholtz problems. An advantageous ACA algorithm may recognize such a block and reduce the

memory storage requirements by utilising only a single coefficient, since there is not any contribution of such a block in solving the problem.

## 4 Numerical Results

In this section the efficiency of the proposed strategy is assessed through numerical results of four different groups of simulations. The first regards the results of a simple benchmark problem whose analytical solution is well known [Pierce (1981)], i.e., a uniform pulsating sphere. The second example is utilised to compare the solution time of a standard BEM formulation using constant boundary elements [Dominguez (1993)] referred as “SBEM”, the old Hierarchical ACA GMRES strategy [Brancati, Aliabadi and Benedetti (2009)] (ORabem) and the new proposed formulation (NRabem). The third example evaluates the resonance frequencies of an aircraft cabin where the surfaces have a different absorbing coefficient and the fourth example simulates the noise generated by an aircraft approaching an airport. In all the example the cardinality is set to 25 and the value of  $\eta$  to 600.

### 4.1 Pulsating Sphere

The analytical solution in terms of the pressure  $p$  at a point with distance  $d$  from the centre of the sphere having radius  $a$  and uniform pulsating velocity  $q_r$  is given as follows [Pierce (1981)]

$$p(d) = \frac{a}{d} q_r \rho_0 c \frac{-ika}{1+ika} e^{ik(d-a)} \quad (22)$$

where  $\rho_0$  is the medium density. To make this study as simple as possible, the pressure is evaluated considering the radius  $a$ , distance  $d$ , normal uniform radial vibrating velocity  $q_r$  and acoustic impedance  $\rho_0 c$  equal to unity.

The mesh of the sphere is composed by 4764 triangular elements with linear variation for geometry and constant for the unknown functions. The effect of a pulsating sphere can be described by the BEM using the Neumann BCs with unitary value for all the boundary elements.

In table 1 the pressure obtained by the analytical solution, the standard BEM approach and by the proposed strategy are shown for seven values of wavenumber, i.e.,  $k=1, 2, 3, 4, 5, 6, 7$ .

The close agreement between the results of both the BEM approaches with the analytical solution prove the proposed approach is accurate.

Table 1: Pressure for a pulsating sphere under prescribed uniform flux for five wave numbers ( $k = 1, 2, 3, 4, 5, 6, 7$ ).

Wave num. $k$	Analytical Solution		Standard BEM		ACA $\mathcal{H}$ -Matrix GMRES	
	Real part	Imag. part	Real part	Imag. part	Real part	Imag. part
1	0.5000	-0.5000	0.4995	-0.5000	0.4997	-0.5002
2	0.8000	-0.4000	0.7996	-0.4000	0.7998	-0.4004
3	0.9000	-0.3000	0.8980	-0.2966	0.8977	-0.3001
4	0.9412	-0.2353	0.9411	-0.2364	0.9417	-0.2358
5	0.9615	-0.1923	0.9608	-0.1929	0.9615	-0.1928
6	0.9730	-0.1622	0.9691	-0.1611	0.9707	-0.1628
7	0.9800	-0.1400	0.9809	-0.1421	0.9811	-0.1406

#### 4.2 Acoustic Scattering from an Absorbing Sphere

In this subsection the solution time between the standard BEM and the old Hierarchical ACA GMRES strategy with the proposed strategy are compared. The problem consists on the acoustic scattering from a sphere with sound absorbing properties illuminated by a plane wave. The sphere radius has unitary radius. The sphere surface has a uniform absorbing coefficient equal to 0.5 and the analysis is performed for a single wave number, i.e.,  $k = 1$ .

Eleven different meshes are used for such a purpose constituted by a different number of elements (Dof): 646, 2112, 3240, 4764, 6351, 8488, 10340, 20232, 28194, 41072, 64452.

Table 2 shows the speed up ratio obtained for setting up the governing matrix and right hand side vector, evaluating the solution, and the total time is calculated as the sum of both the previous CPU time. The speed up ratio is defined as CPU time of both the SBEM or ORabem divided by the CPU time of NRabem.

It can be noted that the maximum Dof for SBEM and ORabem is 10340 and 64452, respectively. This is due to the fact that for more refined meshes the limit of 2GB of the operative system utilised (Windows 7) for each simulation is exceeded.

#### 4.3 Aircraft Cabin Frequency Response

The results of a series of simulations to evaluate the frequency response of an aircraft cabin are presented in this section.

Since aircraft cabins are symmetrical with respect to the middle plane, a panel, simulated with rigid boundary conditions ( $q = 0$ ), can be inserted to reduce the

Table 2: Speed up ration between the SBEM and the ORabem with the NRabem.

Dof of sphere	SBEM/NRabem			ORabem/NRabem		
	Setting Up	Solver	Total	Setting Up	Solver	Total
646	-45.99	2209.93	70.56	28.47	-3.57	26.81
2112	13.00	17298.95	771.17	21.71	5.91	21.01
3240	53.96	36163.48	1595.66	26.90	33.63	27.19
4764	113.12	74432.70	3229.08	30.67	28.27	30.57
6354	179.54	125440.21	5445.69	35.35	31.10	35.17
8488	249.90	203234.85	8869.34	35.85	31.49	35.67
10340	320.30	296316.23	12880.53	39.55	35.89	39.40
20232	-	-	-	44.09	56.34	44.59
28194	-	-	-	47.34	37.41	46.89
41072	-	-	-	49.24	22.18	47.87
64452	-	-	-	-	-	-

computational cost considering only half cabin. Thus, the analysed half model contains two lines of three seats delimited by the ceiling, a lateral panel and the floor, and by two panels one at the front and one at the rear of the cabin. It is included in a cuboid of dimensions  $2 \times 1.9 \times 2.3$  and each line of the seats has dimensions  $0.5 \times 1.35$  m with height 1.054 m. The discretised model is constituted by 11599 nodes and 15392 elements. The maximum size of all the elements is 0.126 m, hence the mesh can deal with frequencies up to 350 Hz.

In order to run a simulation close to a real circumstance the rear and front panel are modeled as soft surfaces ( $u = 0$ ), seats, floor, ceiling, have all been modeled with absorbing coefficients having variable values.

Table 3 reports the absorbing coefficients utilised from 70 Hz to 300 Hz.

Since the absorbing coefficient is a real number, the impedance, being a complex number, cannot be uniquely determined unless a second equation is considered. The proposed equation fixes the impedance phase equal to zero.

The sound inside the cabin is generated by a monopole with unitary strength and located close to the symmetry panel at the point (1.870, 0.250, 1.900).

Figure 4 shows the model representing the aircraft cabin and the monopole source. The symmetry panel has been removed for a better overview. All the other surfaces with same BCs have been alike colourful.

The aircraft cabin response for a frequency range between 70 Hz and 300 Hz is de-

Table 3: Absorbing coefficients of the aircraft model at various frequencies: seats, floor and ceiling.

Frequency Hz	Seats	Floor	Ceiling
70	0.3000	0.1000	0.060
100	0.3535	0.1214	0.1232
130	0.4071	0.1429	0.1864
160	0.4607	0.1642	0.2496
190	0.5143	0.1857	0.3129
220	0.5679	0.2071	0.3761
250	0.6214	0.2286	0.4393
280	0.6750	0.2500	0.5025
300	0.7107	0.2643	0.5446

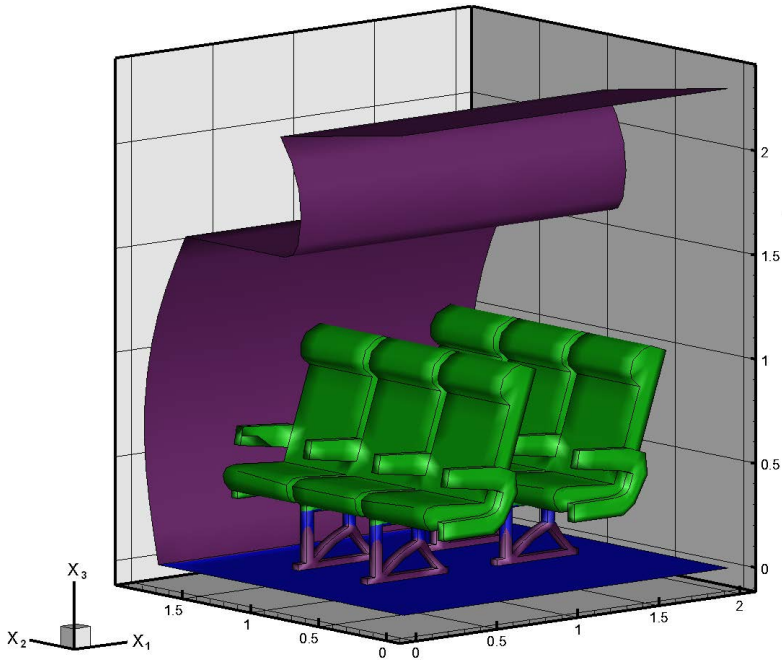


Figure 4: Model representing an aircraft cabin.

pictured in figure 5. In particular the response trend is evaluated at a point placed inside the model away from the anti-node points and located at (0.675, 0.230, 0.900). As evident there are four picks in the range considered which are 80, 108, 138 and 182 Hz.

Figure 6 shows the SPL within the cabin for 80 Hz. As evident the sound source generates two waves with wavelength of half of the cabin length.

#### **4.4 Airplane Approaching an Airport**

In recent years much attention is payed to investigate and reduce the noise pollution generated by airplanes approaching airports, since it can be a profound irritating factor for people who live in proximity of this areas (see figure 7).

This subsection presents the a series of simulations to evaluate the sound pressure level generated by the engine of an aircraft during a landing phase to buildings close to an airport. The noise due by an approaching airplane is generated mainly by five sources, i.e., engines, landing gear, flaps, slats and tail. However, the main contribution to the noise is the engine which, for instance, in a Airbus A340, contributes of about 60% of the total disturbance [Sijtsma and Stoker (2004)].

The proposed example is focused mainly on the noise generated by the engine and it demonstrates that the proposed procedure can be applied also to a large scale external problems common to real industrial simulations.

The problem of reducing the noise level of residential house close to airport is beyond the scope of this paper and more details on this subject can be found in the literature [Ciskowski and Brebbia (1991); Hansen and Snyder (1997)].

The aircraft model utilised in this simulation represents a Dassault Falcon. Its total length aircraft is 18.5 m, its wing span is 22.46 m and its total height is 5.75 m.

The model is discretised with 47,998 constant triangular elements (see figure 8). The sizes of the largest element is 0.23 mm so the maximum frequency that can be applied is around 185 Hz. The frequency of the simulation is 100 Hz.

The surface of the aircraft are modelled as hard ( $q = 0$ ). The noise is generated by vibrating surfaces of the engine. In particular the compressor has a vibrating surface of (1.0, 0.0), the turbine of (1.2, 0.0) and the rest of the covering surface between (0.4, 0.0) and (0.8, 0.0) (see figure 9).

Figure 10 shows the sound pressure level generated by the proposed model at 100Hz.

The houses (see figure 11) are 5 m length, 7 m deep and 3 m height until the roof and 6 m to the top. There are two windows at each later prospect, four on the roof, and one in the front and rear prospect where there are also two entrance doors.

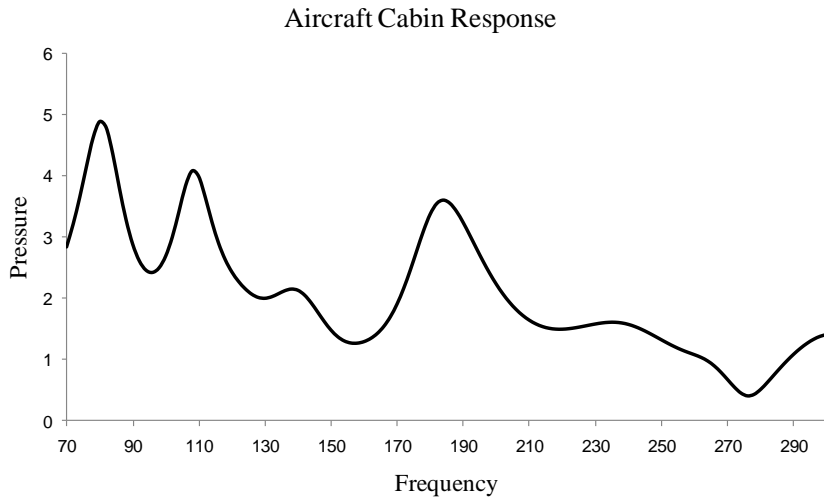


Figure 5: Aircraft model response against the frequencies.

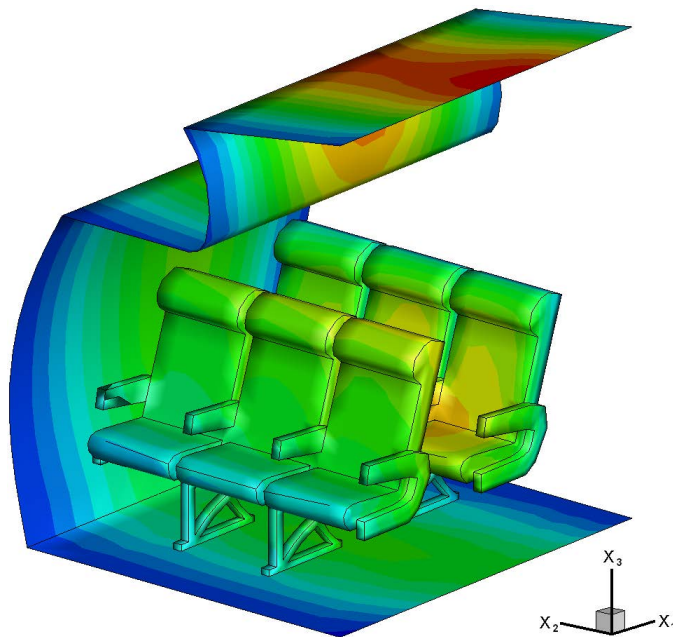


Figure 6: SPL within the cabin at 80 Hz.



Figure 7: Qantas Boeing 747 approaching runway 27L at London Heathrow Airport, England wikipedia.org (2011).

Each of these surfaces has a specific sound absorbing coefficient. In particular, in this simulation the door have a sound absorbing coefficient of 0.1, the wall of 0.01 and the windows of 0.25. Finally, the ground has an absorbing coefficient of 0.4.

The sound pressure level trend generated by the proposed model of the Dassault Falcon approaching an airport is shown in figures 11 and 13 for seven different altitudes from the ground (120, 100, 80, 60, 40, 30, 20 m) at 10 Hz.

## 5 Summary

An improved Hierarchical ACA GMRES approach for solving 3D Helmholtz problems with complex geometries, several degrees of freedom and sound absorbing surfaces has been presented.

This paper described a new procedure for generating the cluster tree. It has been demonstrated that the ACA can be applied to a kernel formed by the linear combination of two asymptotic smooth kernels as in case of mixed Robin conditions. Thus, the memory storage requirement is considerable reduced as well as the CPU time utilised by the GMRES due to the reduction of the number of matrix-vector multiplications.

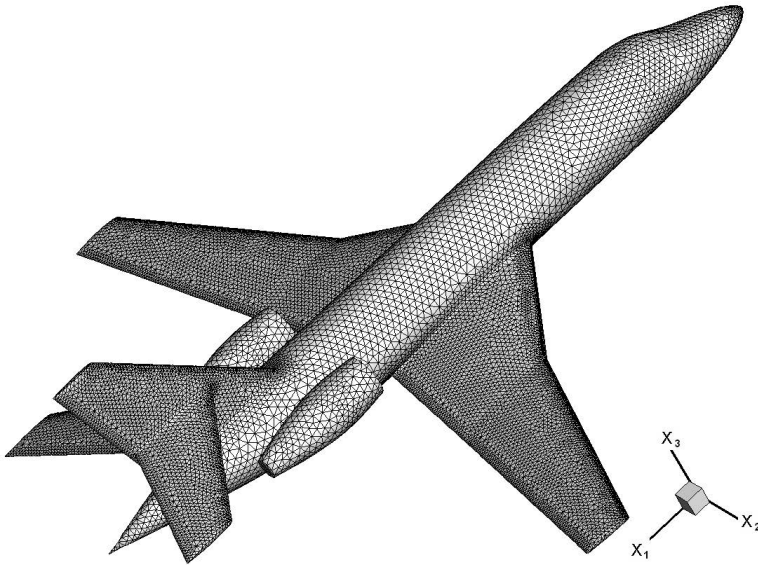


Figure 8: 47,998 triangular elements Dassault Falcon mesh.

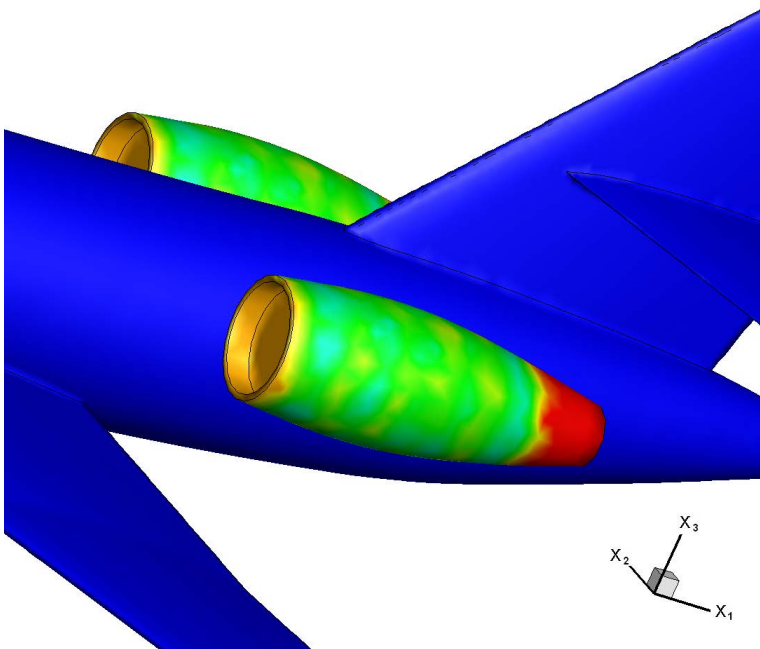


Figure 9: 53,074 triangular elements Dassault Falcon mesh.

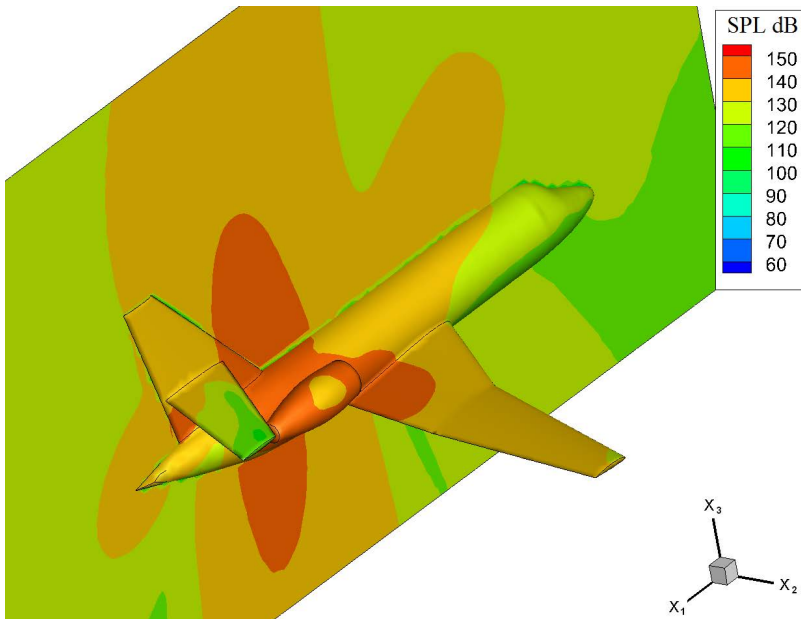


Figure 10: Sound pressure level at 100 Hz generated by a model of a Dassault Falcon.

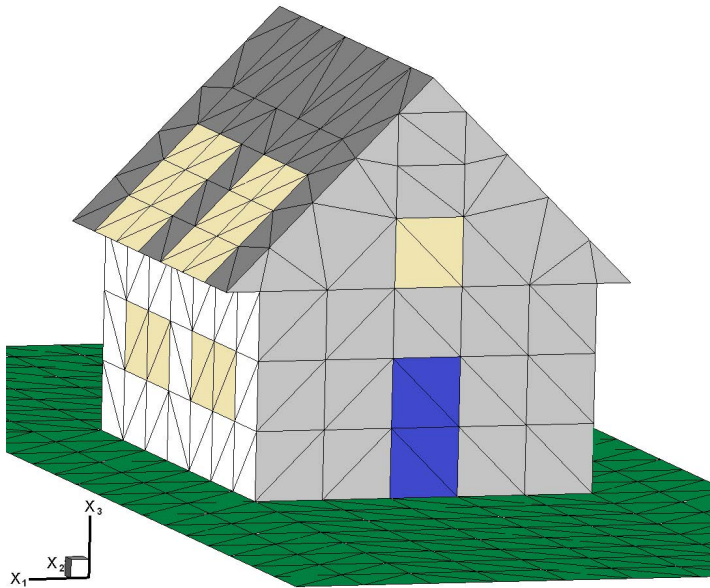


Figure 11: Geometry of the house.

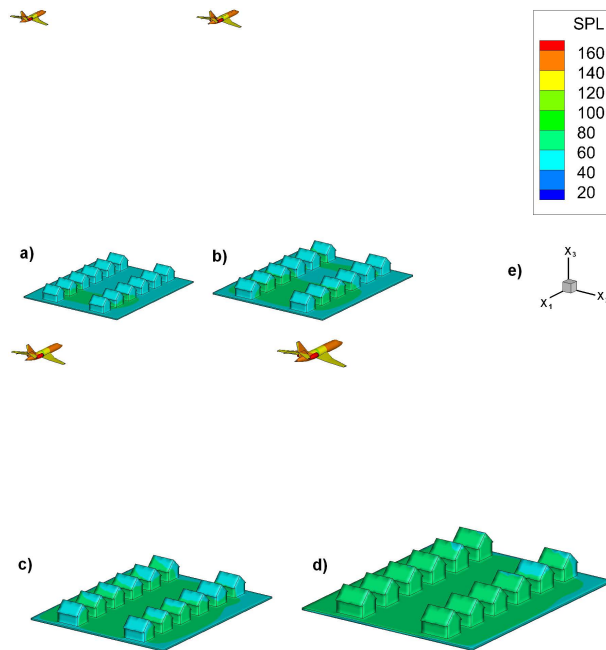


Figure 12: Sound pressure level at 10 Hz generated by a Dassault Falcon approaching in an airport at different altitudes: a) 120 m; b) 100 m; c) 80 m; d) 60 m.

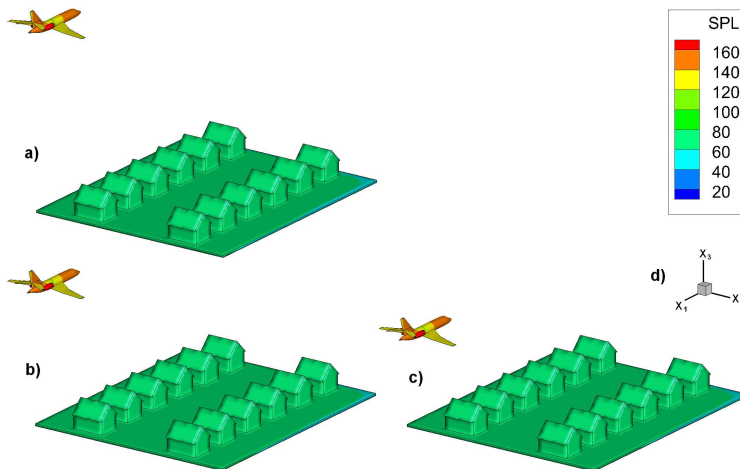


Figure 13: Sound pressure level at 10 Hz generated by a Dassault Falcon approaching in an airport at different altitudes: a) 40 m; b) 30 m; c) 20 m.

Several examples shown the accuracy and the achieved speed up of the proposed strategy. Results of two examples demonstrated the possibility of a direct application to engineering problems.

## References

**Bebendorf, M.** (2000): Approximation of boundary element matrices. *Numerische Mathematik*, vol. 86, pp. 565-589.

**Bebendorf, M.; Rjasanow, S.** (2003): Adaptive low-rank approximation of collocation matrices. *Computing*, vol. 70, no. 1, pp. 1-24.

**Bebendorf, M.; Grzhibovskis, R.** (2006): Accelerating Galerking BEM for linear elasticity using adaptive cross approximation. *Mathematical Methods in the Applied Sciences*, vol. 29, pp. 1721-1747.

**Benedetti, I.; Aliabadi, M. H.; Daví G.** (2007): A fast 3D dual boundary element method based on hierarchical matrices. *International Journal of Solids and Structures*, vol. 45, no. 7-8, pp. 2355-2376.

**Benedetti, I.; Aliabadi, M. H.** (2010): A Fast Hierarchical Dual Boundary Element Method For Three-Dimensional Elastodynamic Crack Problems, *International Journal for Numerical Methods in Engineering*, vol. 84, pp. 1038–1067.

**Börm, S.; Grasedyck, L.** (2000): Hybrid cross approximation of integral operators. *Numerische Mathematik*, vol. 101, no. 2, pp. 221-249.

**Brancati, A.; Aliabadi, M.H.; Benedetti, I.** (2009): Hierarchical Adaptive Cross Approximation GMRES Technique for Solution of Acoustic Problems Using the Boundary Element Method. *CMES*, vol. 43, no. 2, pp. 149-172.

**Brancati, A.** (2010): *Boundary Element Method for Fast Solution of Acoustic Problems: Active and Passive Noise Control*. PhD Thesis, Imperial College London.

**Brancati, A.; Aliabadi, M. H.** (2011): Boundary Element Simulations For Local Active Noise Control Using An Extended Volume. To appear in *EABE: Engineering Analysis with Boundary Elements*, DOI: 10.1016/j.enganabound.2011.06.008.

**Brancati, A.; Aliabadi, M. H.; Mallardo, V.** (2011): A BEM Sensitivity Formulation For 3D Active Noise Control. To appear in *International Journal for Numerical Methods in Engineering*.

**Buchau, A.; Rucker, W. M.; Rain, O.L.; Rischmüller, V.; Kurz, S.; Rjasanow, S.** (2003): Comparison Between Different Approaches for Fast and Efficient 3-D BEM Computations. *Ieee Transactions On Magnetics*, vol. 39, no. 3, pp. 1107-1110.

- Carrier, J.; Greengard, L.; Rokhlin, V.** (1988): A fast adaptive multipole algorithm for particle simulations. *SIAM J. Sci. Statist. Comput.* vol. 9, pp. 669-686.
- Ciskowski, R. D.; Brebbia, C. A.** (1991): *Boundary Element Methods in Acoustics*. Computational Mechanics Publications Elsevier Applied Science.
- Crotty, J. M.** (1982): A block equation solver for large unsymmetric matrices arising in the boundary integral equation method. *International Journal for Numerical Methods in Engineering*, vol. 18, no. 7, pp. 997-1017.
- Dominguez, J.** (1993): *Boundary Elements in Dynamics*. Computational Mechanics Publications.
- Greengard, L.; Rokhlin, V.** (1987): A fast algorithm for particle simulations, *J. Comput. Phys.*, vol. 73, pp. 325-348.
- Hackbusch, W.; Nowak, Z.** (1989): On the fast matrix multiplication in the boundary element method by panel clustering. *Numerische Mathematik*, vol. 73, pp. 207-243.
- Hackbush, W.** (1999): A sparse matrix arithmetic based on H-matrices. Part I: introduction to H-matrices. *Computing*, vol. 63, pp. 89-108.
- Hackbush, W.; Khoromskij, B.N.** (2000): A sparse matrix arithmetic. Part II: application to multidimensional problems. *Computing*, vol. 64, pp. 21-47.
- Hansen, C. H.; Snyder, S.D.** (1997): *Active control of noise and vibration*. Spon.  
[http://en.wikipedia.org/wiki/File:Qantas\\_b747\\_over\\_houses\\_arp.jpg](http://en.wikipedia.org/wiki/File:Qantas_b747_over_houses_arp.jpg), May 2010.
- Kane, J. H.; Kumar, K.** (1990): An Arbitrary Condensing, Noncondensing Solution Strategy for Large Scale, Multi-Zone Boundary Element Analysis. *Comp. Methods Appl. Mech. Eng.*, vol. 79, pp. 219-244.
- Leung, C. Y.; Walker, S. P.** (1997): Iterative solution of large three dimensional BEM elastostatic analyses using the GMRES technique. *International Journal for Numerical Methods in Engineering*, vol. 40, pp. 2227-2236.
- Mallardo, V.; Aliabadi, M. H.; Brancati, A.; Marant, V.** (2011): Noise control in the aircraft cabin. To appear in *Aerospace Science and Technology*.
- Mansur, W. J.; Araújo, F. C.; Malaghini, J. E. B.** (1992): Solution of BEM systems of equations via iterative techniques. *International Journal for Numerical Methods in Engineering*, vol. 33, no. 9, pp. 1823-1841.
- Merkel, M.; Bulgakov, V.; Bialecki, R.; Kuhn, G.** (1998); Iterative solution of large-scale 3D-BEM industrial problems. *Engineering Analysis with Boundary Elements*, vol. 2, pp. 183-197.

**Pierce, A.D.** (1981): Acoustic: an introduction to its Physical Principles and Applications. *McGraw Hill, New York*.

**Rigby, R. H.; Aliabadi, M. H.** (1995): Out-of-core solver for large, multi-zone boundary element matrices. *International Journal for Numerical Methods in Engineering*, vol. 38, no. 9, pp. 1507-1533.

**Rokhlin, V.** (1983): Rapid solution of integral equations of classical potential theory. *J. Comput. Phys.*, vol. 60, pp. 187-207.

**Saad, Y.; Schultz, M. H.** (1986): GMRES: A generalized minimal residual algorithm for solving nonsymmetric linear systems. *SIAM J. Sci. Stat. Comput.*, vol. 7, no. 3, pp. 856-869.

**Sijtsma, P., Stoker, R.W.** (2004): Determination of Absolute Contributions of Aircraft Noise Components using Fly-Over Array Measurements. AIAA Paper 2004-2958, 10th AIAA/CEAS Aerocoustics Conference, Manchester, UK, 10-12 May.

**Von Estorff, O.; Rjasanow, S.; Stolper, M.; Zalesk, O.** (2005): Two efficient methods for a multifrequency solution of the Helmholtz equation. *Computing and Visualization in Science*, vol. 8, pp. 159-167.

**Wang, H. T.; Hall, G.; Yu, S. Y.; Yao, Z. H.** (2008): Numerical Simulation of Graphite Properties Using X-ray Tomography and Fast Multipole Boundary Element Method. *CMES: Computer Modeling in Engineering & Sciences*, vol. 37, no. 2, pp. 153-174.

**Wang, H. T.; Yao, Z. H.** (2008): A Rigid-fiber-based Boundary Element Model for Strength Simulation of Carbon Nanotube Reinforced Composites. *CMES: Computer Modeling in Engineering & Sciences*, vol. 29, no. 1, pp. 1-14.

**Wrobel, L. C.; Aliabadi, M. H.** (2002): The boundary Element Method. Two volumes set. *New Jersey: UK JOHN WILEY*.